Jordan Journal of Energy
Volume 2, Number 1, 2024

ISSN (Online): 2790-7678
ISSN (Print): 2790-766X

Jordan Journal of Energy (JJE)
Journal Homepage: http://dsr.mutah.edu.jo/index.php/jje
JEE an official peer review journal of Mutah University,

A Triple Band Flexible Antenna based on Asymmetric Spiral Split Rings Coupled to External Loop

Anwar Tarawneh
Mutah University, Jordan
Email: Anwar1989@mutah.edu.jo

Received 18th, Jan 2024; Accepted 2nd, Apr 2024

ABSTRACT. *In this paper a small flexible antenna is designed and proposed for implantable applications in the 401-406 MHz Medical Device Radio Communication Service (MedRadio), 433-434.8 MHz and 2.4-2.5 GHz Industrial Scientific Medical (ISM) bands. The proposed antenna has a unique structure exploiting spiral split rings to achieve both miniaturization and excellent impedance matching (S11< -10 dB) within the 401-406 and 433-434.8 MHz bands. For resonance in the 2.4-2.5 GHz ISM band, the spiral split rings are coupled with an external feeding loop ring. This comprehensive band coverage enables the antenna to facilitate data transfer, wireless power charging and saving. The proposed antenna has obtained a gain value of -22.44, -22.07, and -25.66 dBi at 403 MHz, 433 MHz, and 2.45 GHz respectively in a simplified body model of 400×50×50 mm^3. Additionally, this antenna design has demonstrated robust performance in different simplified body models. Furthermore, the antenna's simple structure makes it a strong candidate for applications in the field of biomedical implants.*

Keywords: ISM; MedRadio; Split rings.

1. Introduction. Implantable medical devices play a crucial role in enhancing and elevating the quality of life for millions of individuals across the globe [1]. These devices have the ability to observe a patient's psychological information and transmit it to an external source [2]. Lately, these implantable devices have been applied in abroad spectrum of beneficial applications, such as health care monitoring, capsule endoscopy, post-surgery checkups, cardiac pacemaker, defibrillators, blood glucose monitoring, blood sugar level monitoring, cochlear and retinal implants [3].

In order to establish a wireless communication between the biomedical device and an external receiving station outside the human body an implantable biomedical antenna is implanted within the human body 4.

Designing implantable antennas has become a complex challenge, and requires the satisfaction of many contradicting conditions simultaneously including the size restrictions, biocompatibility issue, specific absorption rate (SAR) to ensure patient safety [3], tissue coupling, acceptable communication ability, bandwidth, licensing of operating frequencies, sufficient radiation efficiency and variation of dielectric properties of tissues, which disturb the antenna capabilities [3], [5-6]. The implantable antenna is also

preferred to work for multiple frequency bands in order to support other functionalities such as wireless power transfer and power saving [7].

A lot of work has already been proposed to tackle the aforementioned challenges. In [8], a compact broadband circularly polarized implantable antenna was proposed to work for the 401-406 MHz band. It had a size of $57.76\ \text{mm}^3$ and a gain value of -31.2 dBi. Another implantable antenna was also proposed in [9] to work at the same frequency band for health monitoring. That antenna was $736\ \text{mm}^3$ in size. It also obtained a gain value of -6.78 dBi. The designs in [10-11] obtained a broad bandwidth covering both of the 401-406 MHz MedRadio and 433-434.8 MHz ISM bands. Other designs in [12-13] obtained a dual band (401-406 MHz MedRadio and 2.4-2.5 GHz ISM) coverage. Triple band coverage were also obtained in [14-15]. Despite these designs obtained multi-band coverage. They were rigid. Also, some of them were proposed for higher frequency bands in which attenuation is relatively large or for unlicensed frequency bands.

Flexible antennas provide many attractive features for implantable applications which include light weight, conformity to many structures. Also, they are usually very thin which leaves larger internal space for other components inside the implantable device. In [16-19] a set of flexible implantable antennas were proposed. These antennas generally obtained a small size which was smaller than $3\ mm^3$ for the design in [20], they worked in either congested (2.45 GHz ISM bands) or high frequency (5.8 GHz) bands at which the human body attenuation is large. Moreover, all of these antennas worked for one frequency band only. The design in [21] had also proposed to work for a single band at 915 MHz. Dual-band designs were proposed in [22-24]. Triple band designs were proposed in [25] which worked at 2.45, 4.8 and 5.8 GHz. The antenna in [26] obtained 401-406 MHz, 902-928 MHz and 2.40-2.48 GHz band coverage. However, it obtained a gain of -41.3 dBi only at 402 MHz. The design proposed in [27] worked for 402 MHz, 915 MHz and 1.2 MHz. The antenna in [28] obtained a five band coverage. However, its design was based on integrating complementary split rings to a loop. This made its structure complex and resulted in discrepancies between measured and simulated results.

Considering this, there is a need for a new kind of flexible and multi-band antenna design. This design is required to overcome the shortcomings seen in earlier designs while maintaining a simple structure. Hence, a new flexible antenna is proposed in this paper. The proposed antenna worked for triple (401-406 MHz MedRadio, 433-434.8 MHz and 2.4-3.5 GHz ISM) bands. It can be bent around cylindrical implants with a radius of 5 mm and a height of 20 mm. The design is simple and showed a good performance in different body models as will be shown in this paper.

This paper is structured as follows: First, the structure and design of the proposed antenna are presented. This is followed by an evaluation and validation of the antenna performance. Conclusions are finally summarized in the final Section.

2. Structure and Design. This section provides an overview of the parameters and structure of the proposed antenna design. The antenna is created using Microwave Computer Simulation Technology (CST) [29] employing hexahedral meshes and transient time solver.

ISSN (Online): 2790-7678
ISSN (Print): 2790-766X

Figure 1 illustrates the suggested antenna design, which consists of a pair of elliptical split rings positioned in two opposing orientations: vertical and horizontal. The inner vertical split ring is linked to the outer horizontal split ring, forming a spiral configuration. This serves two purposes: 1) enhancing the current path to facilitate antenna miniaturization and 2) amplifying the near magnetic field, thereby increasing the gain of implantable antenna, as described in Eq. (1) [3]:

$$G_{con} = \frac{4\pi\sqrt{(\omega\mu)/(2\sigma)}\left(|H|de^{(d/\delta)}\right)^2}{R_r(I_i)^2} \quad (1)$$

The tissue permeability is denoted as μ[H/m], while μ[H/m] represents the magnitude of the magnetic field intensity taken in the maximum field direction of the antenna under consideration at distance $d[m]$,, $R[\Omega]$ signifies the intrinsic resistance, δ represents the skin depth, $R_r[\Omega]$ denotes the radiation resistance and $I_i[A]$ stand for the input current.

The rings that forming the spiral are coupled to extra split rings, as depicted in figure 1. This coupling not only achieves further miniaturization of the antenna but also enhances the antenna near magnetic field [10]. A detailed summary of the overall design parameters for the proposed antenna is outlined in table 1.

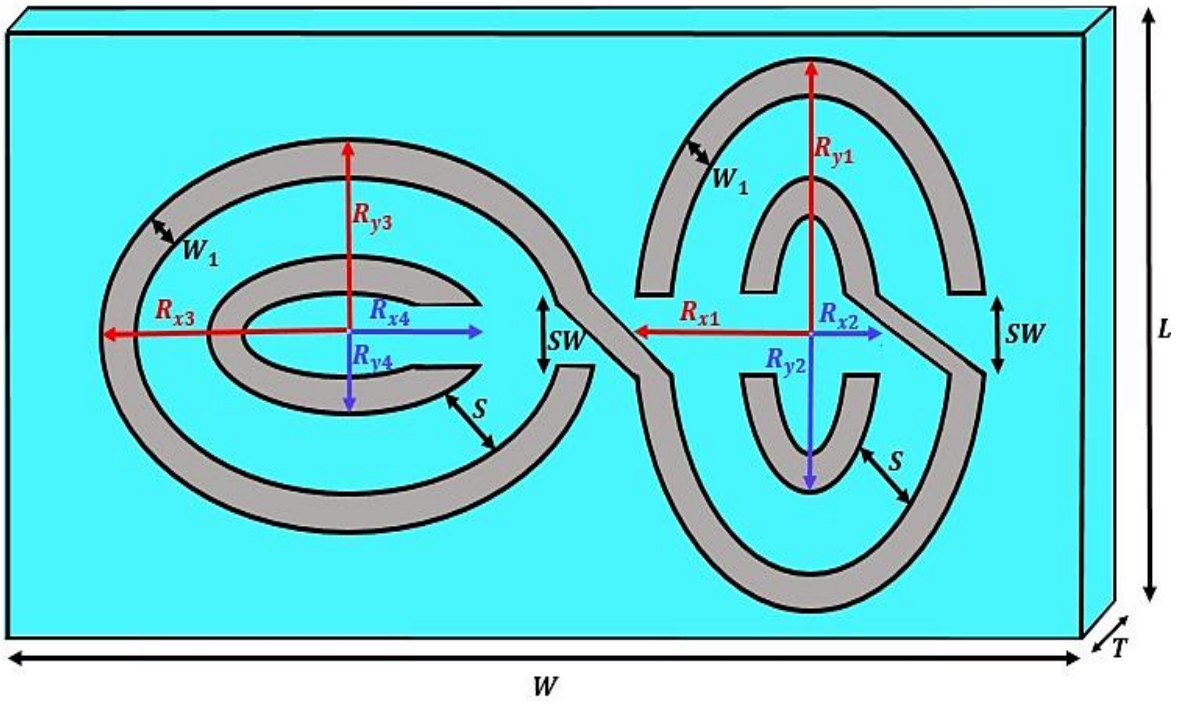

FIGURE. 1. Geometric design of the proposed antenna

TABLE 1. Optimized parameters of the proposed antenna.

Parameters	Symbol	Values (mm)	Parameters	Symbols	Values (mm)
Substrate length	L	20.0	x-radius for outer horizontal ring	R_{x3}	7.00
Substrate width	W	30.0	x-radius for inner horizontal ring	R_{x4}	4.00
Split width	SW	2.00	y-radius for outer vertical ring	R_{y1}	7.00
Spacing between Splits	S	2.00	y-radius for inner vertical ring	R_{y2}	4.00
Ring width	W_1	1.00	y-radius for outer horizontal ring	R_{y3}	5.00
x-radius for outer vertical ring	R_{x1}	5.00	y-radius for inner horizontal ring	R_{y4}	2.00
x-radius for inner vertical ring	R_{x2}	2.00	Thickness of substrate	T	2

The flexible antenna is constructed using s substrate with a relative permittivity (ε_r) of 3. It is capable of being bent around a cylindrical implant with a radius of 5 mm and a length of 20 mm. Figure 2 illustrates the antenna's configuration around the cylindrical implant.

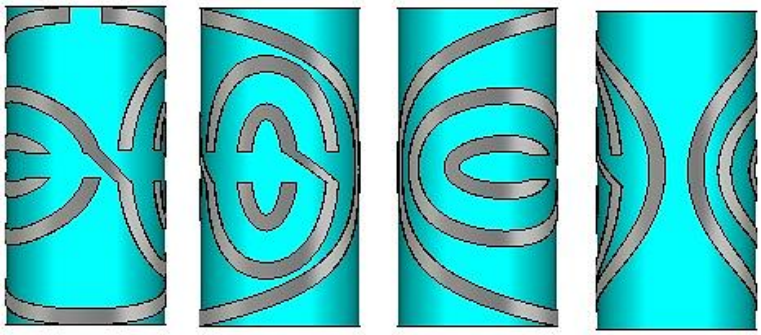

(a) (b) (c) (d)

FIGURE. 2. Physical layout model of the designed antenna: (a) Front view, (b) Right view, (c) Left view, and (d) Back view.

The implant's surrounding antenna is placed at the center of a cylindrical body model constructed with muscle. This muscle tissue exhibits heterogeneity with diverse dielectric properties at frequencies of 403 MHz, 433 MHz, and 2.45 GHz, as outlined in table 2 [30-31]. Figure 3 illustrate the body model along with its overall dimensions.

ISSN (Online): 2790-7678
ISSN (Print): 2790-766X

TABLE 2. Dielectric properties of muscles at 403 MHz, 433 MHz, and 2.45 GHz [30-31].

Frequency (MHz)	Relative permittivity	Conductivity [S/m]	Loss tangent	Mass density (kg/m^3)
403	57.104	0.7970	0.6226	
433	56.873	0.8048	0.5874	1041
2450	52.729	1.738	0.2419	

The selection of spacing between the rings and the split width (spacing between the edges of the rings) has been methodically made to achieve resonance at the three specific frequency bands of interest. This careful consideration is geared towards maximizing both gain and radiation efficiency, ensuring optimal performance of the antenna.

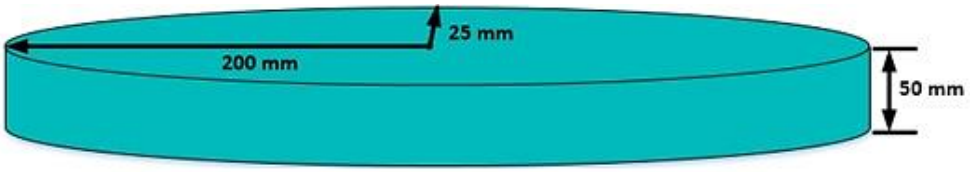

(a)

(b)

FIGURE. 3. (a) simplified body model, (b) Schematic diagram of the proposed antenna implanted into the muscle model.

2.1 Effect of Design Parameters on the Antenna Performance. This section explores the impact of both the split width and the spacing between the splits on the resonant frequency. This investigation is promoted by the expectation that these two parameters play a central role in determining the overall impact.

2.1.1 Effect of Spacing between Splits (S). Figure 1 illustrates the parameter under consideration, depicting the separation between two metallic rings separated by a dielectric material. This configuration mimics a capacitor with an equivalent capacitance, which can be determined using the formula outlined by [32]:

$$C_c = \frac{4\pi\varepsilon}{\frac{1}{R_{Y4}} - \frac{1}{R_{Y3}}}$$

$$= \frac{4\pi\varepsilon R_{Y3}R_{Y4}}{S} \quad (2)$$

of which $(R_{Y3} - R_{Y4})$ represents S.

Increasing (S) is predicted to cause a decrease in effective capacitance, consequently shifting the resonance frequency upward [33].

$$f_r = \frac{1}{2\pi\sqrt{LC_c}} \quad (3)$$

where L (H) is the effective inductance.

The results of the reflection coefficient, reflecting a 1mm reduction in spacing, are depicted in figure 4.

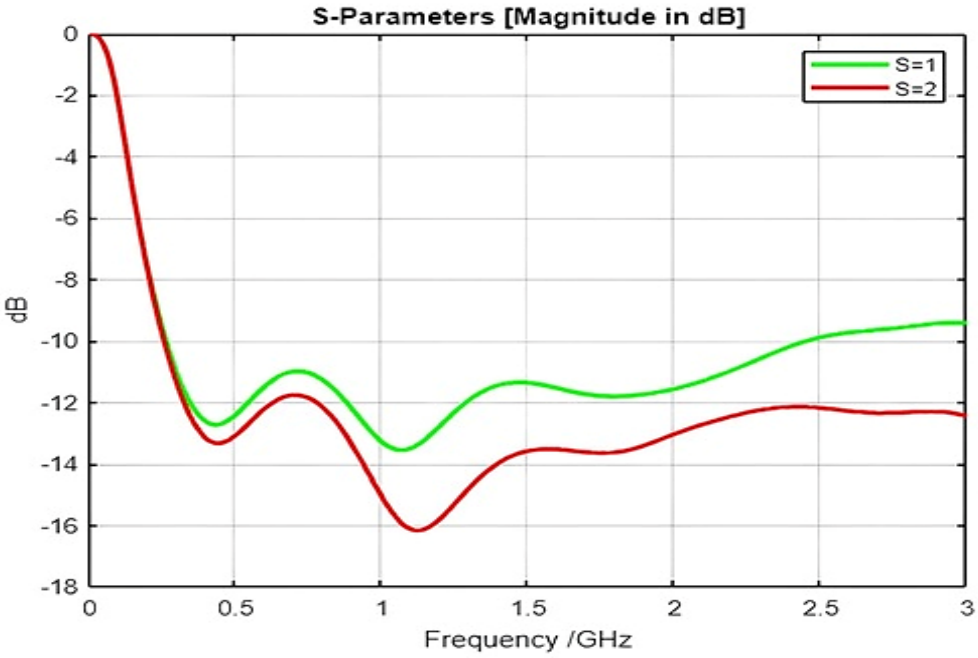

FIGURE. 4. Simulated S11(dB) of the proposed antenna for S=1 and 2 mm.

The illustration clearly shows that a 1 mm decrease in spacing results in a downward shift of the resonant frequency, specifically by 3 MHz. However, this shift is relatively small due to the constrained

ISSN (Online): 2790-7678
ISSN (Print): 2790-766X

range of variations in S limited by the available structure. As depicted in the figure, enhancing the spacing between the rings has contributed to an enhanced matching. A reduction of 1 mm in the spacing also results in a decrease in antenna gain by 0.14 dBi. This reduction is attributed to the increased capacitive effect, as previously detailed.

2.1.2 Effect of Split Width (SW). This spacing indicates the distance between the parallel plates of a capacitor, for which the capacitance (C_P (F)) can be determined as [33]:

$$C_P = \frac{\varepsilon A}{SW} \tag{4}$$

where A (m^2) is the plate area.

A decrease of 1 mm in SW causes the resonant frequency to shift downwards by a round 12 MHz, primarily attributed to increases in C_P. Increasing the capacitance also corresponds to a decrease in gain by 0.13 dBi. This effect is observed only within the lower frequency band (401-406 MHz). Nevertheless, this decrease remains negligible, mainly due to the compact dimensions of the split width. The results of the reflection coefficient, reflecting a 1mm reduction in SW, are depicted in figure 5.

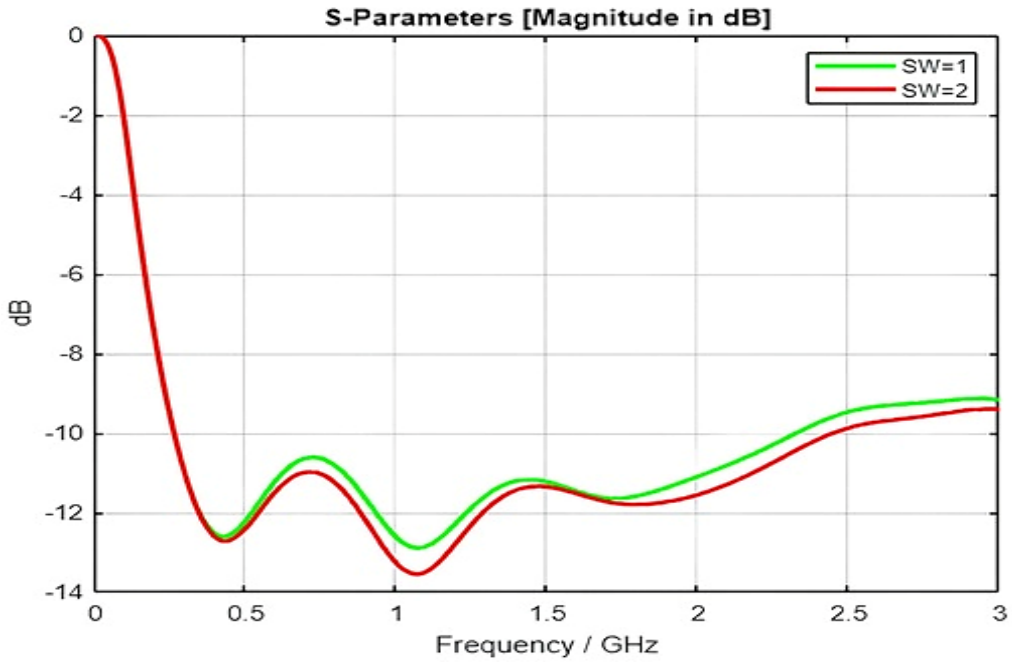

FIGURE. 5. Simulated S11(dB) of the proposed antenna for SW=1 and 2 mm.

3. The Antenna Performance. This section involves the evaluation of the antenna's reflection coefficient, gain, radiation efficiency, radiation pattern, and Specific Absorption Rates (SAR). The

performance is further confirmed through testing on different body models, accompanied by the calculation of a detailed link budget for a comprehensive evaluation.

3.1 The Reflection Coefficient. The antenna reflection coefficient is presented in figure 6, demonstrating a robust matching impedance (S11< -10 dB) across all designated frequency bands.

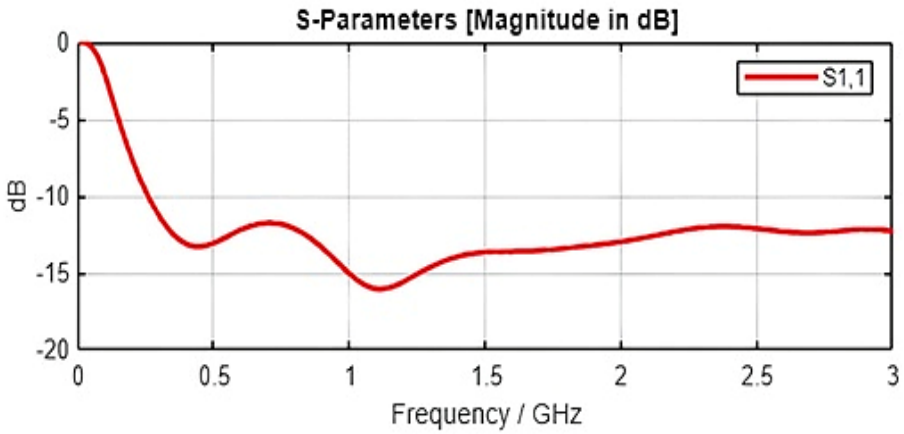

FIGURE. 6. Simulated S11(dB) of the proposed antenna

3.2 The Gain and Radiation Efficiency. Table 3 summarizes the simulated maximum 3D gain and radiation efficiency for the central frequencies across all designated frequency bands. The results indicate that as the frequency increases, both gain and radiation efficiency exhibit an increase at 433 MHz compared to 403 MHz. This is attributed to the antenna being electrically larger at 433 MHz, while human body losses remain relatively constant. Conversely, at 2.45 GHz, there is a decrease in both gain and radiation efficiency, primarily due to higher human body losses at this frequency band.

TABLE 3. Results of maximum 3D gain and radiation efficiency at 403 MHz, 433 MHz, and 2.45 GHz extracted from simulation.

Frequency (MHz)	Gain (dBi)	Radiation Efficiency (dB)
403	-22.44	-24.85
433	-22.07	-24.65
2450	-25.66	-29.66

3.3 Validation in a multilayer Body Model. The simulation of the antenna also involved incorporating it into a multilayer body model, as depicted in figure 7. This model consists of layers of additional fat and skin surrounding the muscle layer, where each fat and skin layer is 4 and 3 mm, respectively. The

ISSN (Online): 2790-7678
ISSN (Print): 2790-766X

corresponding dielectric properties of fat and skin for each frequency band are outlined in table 4 [30-31].

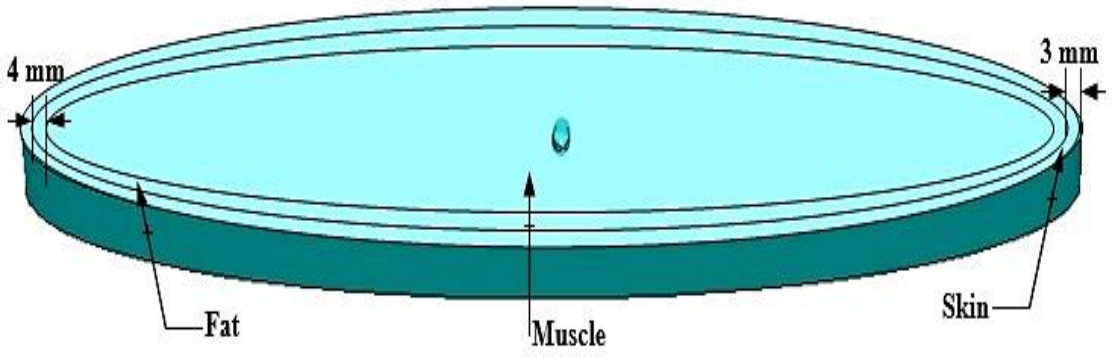

FIGURE. 7. Schematic diagram of the proposed antenna implanted into a multi-layer body model.

TABLE 4. Dielectric properties of fat and skin at 403 MHz, 433 MHz, and 2.45 GHz [30-31].

Body model	Frequency (MHz)	Relative permittivity	Conductivity [S/m]	Loss tangent	Mass density (kg/m^3)
Fat	403	5.5785	0.4116	0.3291	950
	433	5.5667	0.0416	0.3106	
	2450	5.2801	0.1045	0.1452	
Skin	403	46.718	0.6893	0.6581	1010
	433	46.079	0.7019	0.6323	
	2450	38.007	1.464	0.2826	

The depicted reflection coefficient for this case is illustrated in figure 8. As evident from the graph, the antenna exhibits a deep S11 below -10 dB across all the designated frequency bands. In this simulation, the maximum 3D gain is -29.2 dBi, marking a 0.4 dBi reduction compared to the single-layer body model case. This reduction is attributed to reflection losses occurring at the boundaries between the muscle-fat and fat-skin layers.

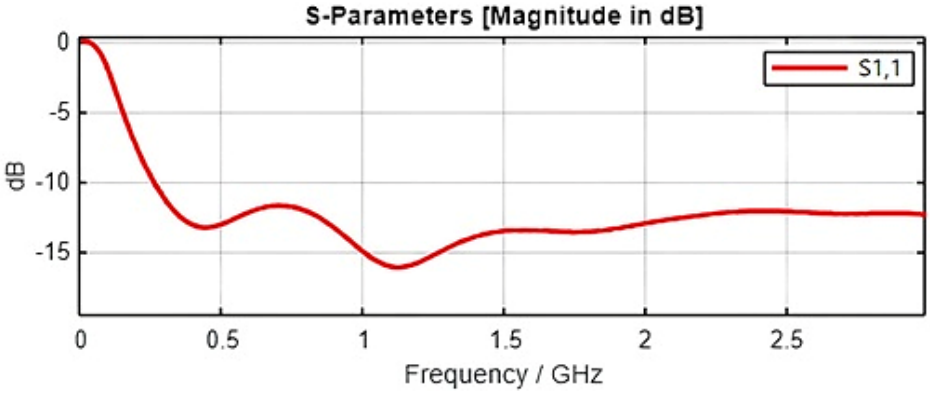

FIGURE. 8. Simulated S11 results for the proposed antenna in the multilayer body

3.4 Link Budget Calculations. The results obtained are utilized in computing the link budget of actual implanatble applications [10], with the relevant link parameters outlined in table 5.

TABLE 5. Link budget parameters of the proposed antenna.

Link parameter	Symbol and Unit	Value		
Frequency	f (MHz)	403	433	2450
Input power to the antenna	P_{tx} (dBm)		0	
Gain of the transmitting antenna	G_{tx} (dBi)	-22.44	-22.07	-25.66
Receiver sensitivity	P_{rx} (dBm)		-99	
Gain of the receiving antenna	G_{rx} (dBi)		2.13	
Link Margin	LM (dB)		5	

The distance over which the proposed antenna communicate is calculated using the following link budget equation [10]:

$$P_{rx} = P_{tx} + G_{tx} + G_{rx} - Loss - LM \tag{5}$$

where P_{tx} (dBm) is the input power to the antenna at the transmission end, G_{tx} (dBi) representing the gain of the transmitting antenna, G_{rx} (dBi) indicating the gain of the receiving antenna, $Loss$ (dB) accounting for the overall loss, and LM (dB) representing the link margin.

The loss ($Loss$) in dB is computed by [10]:

ISSN (Online): 2790-7678
ISSN (Print): 2790-766X

$$Loss = L_p + e_p + ML_{TX} + ML_{RX} \quad (6)$$

where L_p represents the path-loss, e_p represents the polarization mismatch factor, and ML_{TX} (dB) indicates the transmitter impedance mismatch losses and ML_{RX} (dB) is the receiver impedance mismatch losses. In this context e_p, ML_{RX}, ML_{TX} are assumed to be zero.

The path loss (L_p) can be determined by the following formula [28]:

$$L_p(dB) = 10nlog_{10}\left(\frac{d}{d_0}\right) + 10nlog_{10}\left(\frac{4\pi d_0}{\lambda_0}\right) + S \quad (7)$$

where n is the path-loss exponent typically between 1 and 3 and for the worst case of none-line-of-sight (NLOS) n is equals to 3, d (m) is the $T_x - R_x$ distance, λ_0 (m) is the free-space wavelength, d_0 (m) is a reference distance which is assumed to be 1 m and S (dB) is the random scatter around the mean which is assumed to be zero.

The summarized results are outlined in table 6.

TABLE 6. The effective communication distances for the proposed antenna at 403 MHz, 433 MHz, and 2.45 GHz

Frequency (MHz)	**Distance of communication (m)**
403	16.94
433	16.22
2450	2.18

The results presented in the table indicate a decrease in communication distance with an increase in frequency, primarily attributed to increase in propagation losses. Nevertheless, the antenna remains effective for distances exceeding 2 m, demonstrating its suitability for supporting indoor healthcare applications.

The antenna exhibits an omnidirectional radiation patter, with its maximum radiation occurring in the off-body direction. In figure 9, the three- dimensional radiation pattern of the proposed antenna at specified frequencies is illustrated. At 2.45 GHz, the antenna's radiation pattern undergoes a directional change due to variations in electrical size. Despite this alteration, the maximum radiation continues to occur away from the human body, aligning with the antenna's intended direction.

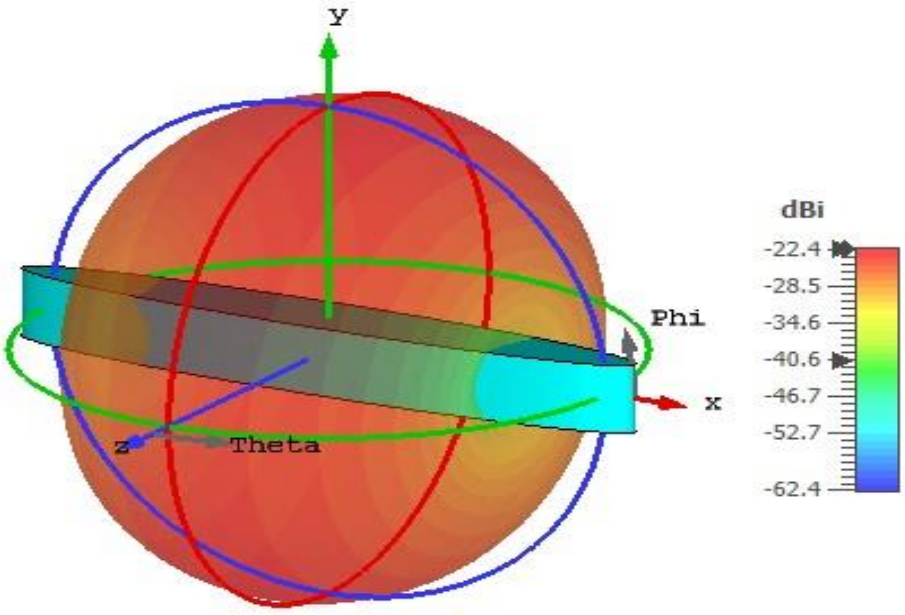
Y
Phi
x
z
Theta
dBi
-22.4
-28.5
-34.6
-40.6
-46.7
-52.7
-62.4

(a)

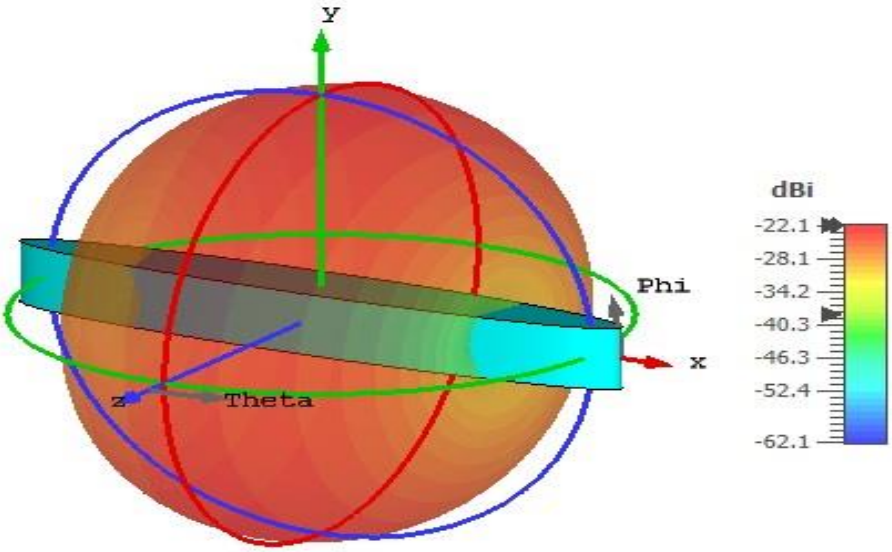
Y
Phi
x
z
Theta
dBi
-22.1
-28.1
-34.2
-40.3
-46.3
-52.4
-62.1

(b)

ISSN (Online): 2790-7678
ISSN (Print): 2790-766X

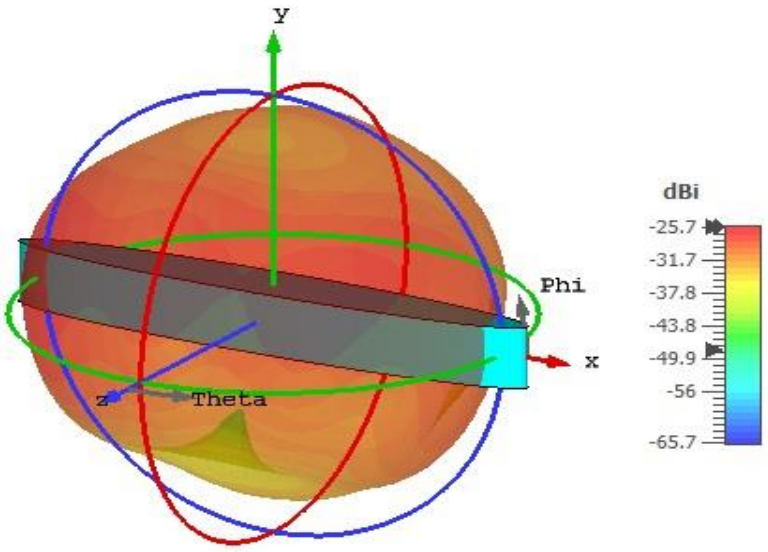

(c)

FIGURE. 9. 3-D far-field gain radiation patterns of the proposed antenna at: (a) 403 MHz, (b) 433 MHz, and (c) 2.45 GHz.

3.5 Specific Absorption Rate (SAR) Analysis. It is crucial to determine the Specific Absorption Rate SAR (W/kg) for antennas implanted in human body tissues to guarantee that the antenna's radiation does not pose any harm to the neighboring body tissues [4], [14]. The SAR level depends on several factors, including the conductivity $\sigma(S/m)$, Near electric field intensity $|\vec{E}|\,(V/m)$, and mass density $\rho\ (kg/m^3)$ [34]:

$$SAR = \frac{\sigma|\vec{E}|^2}{2\rho} \tag{8}$$

In this section, the maximum 1-g SAR has been calculated using Microwave CST for each center frequencies within the bands of interest. The summarized results are outlined in Table 7.

TABLE 6. Max 1-g SAR (W/kg) at 403 MHz, 433 MHz, and 2.45 GHz.

Frequency (MHz)	**Max 1-g SAR (W/kg)**
403	282.34
433	301.57
2450	438.28

The results in the table indicates a direct correlation between SAR values and frequency, with an upward trend attributed to heightened attenuation losses associated with the increasing conductivity at higher frequencies. The calculation of the maximum allowable input power for the antenna relies on

these SAR results. Consequently, the antenna can operate safely with a power input of up to 3.65 mW, ensuring compliance with SAR limits (max 1-g SAR<1.6 W/Kg).

4. Conclusion. This paper details the development of a flexible antenna specifically designed for implantable applications, targeting frequency bands such as MedRadio (401-406 MHz), 433-434.8 MHz, and the (2.4-2.5 GHz) ISM bands. The antenna incorporates spiral split rings to minimize it size and enhance matching across all intended frequency bands. Notably, this antenna boasts a wide bandwidth, making it well-suited for diverse functionalities like data transfer, wireless power charging, and power saving capabilities. In terms of performance, the antenna demonstrates excellent radiation characteristics, ensuring reliable operation at distances exceeding 2 m. Furthermore, it maintains robust performance across various simplified body models while adhering to SAR limitations, with a maximum input power of up to 3.65 mW. The attractive attributes of simplicity, flexibility, strong radiation characteristics, extended communication range, and robust performance, position this antenna as a promising choice for implantable healthcare applications.

Acknowledgment. I would like to extend my sincere appreciation to the anonymous reviewers who dedicated their time and expertise to thoroughly assess and provide insightful feedback on this paper. Their constructive comments and valuable suggestions have played a crucial role in enhancing the quality and clarity of the paper.

REFERENCES

[1] A. Kiourti and K. S. Nikita, A review of implantable patch antennas for biomedical telemetry: Challenges and solutions [wireless corner], *IEEE Antennas Propagat*. Mag., vol. 54, no. 3, pp. 210-228, 2012.

[2] N. Malik, T. Ajmal, P. Sant and M. Ur-Rehman, A compact size implantable antenna for bio-medical applications, *2020 International Conference on UK-China Emerging Technologies. IEEE*, 2020.

[3] A. Tarawneh, A survey on implantable antennas for far-feild betelemetry applications, *Jordan Journals of Electrical Engineering*, vol. 6, no. 1, pp. 1-23, 2020.

[4] R. Nehra and N. Raghava, Highly compact triple ring slotted circular polarized implantable antenna for bio-medical applications, *In: 2021 6th International Conference on Signal Processing, Computing and Control (ISPCC). IEEE*, pp. 186-190, 2021.

[5] M. Zada and H. Yoo, A miniaturized triple-band implantable antenna system for bio-telemetry applications, *IEEE Transactions on Antenna and Propagation*, vol. 66, no. 12, 2018.

[6] I. Ali Shah, M. Zada and H. Yoo, Design and analysis of a compact-sized multiband spiral-shaped implantable antenna for scalp implantable and leadless pacemaker systems, *IEEE Transactions on Antenna and Propagation*, vol. 67, no. 6, 2019.

ISSN (Online): 2790-7678
ISSN (Print): 2790-766X

[7] A. Basir and H. Yoo, Efficient wireless power transfer system with a miniaturized quad-band implantable antenna for deep-body multitasking implants, *IEEE Transactions on Microwave Theory and Techniques,* vol. 68, no. 5, 2020.

[8] D. Nguyen, D. Nguyen and A. Seo, A compact braodband circulary polarized patch antenn using ladder slots and grounded capacitors for Medradio-band applications, *in IEEE Access,* vol. 11, pp. 63997-64004, 2023.

[9] C. -L. Yang, C. -L. Tsai, K. -T. Cheng and S. -H. Chen, Low-invasive implantable devices of low-power consumption using high-efficiency antenna for cloud helath care, *IEEE Journal on Emerging and Selected Topics in Circuits and Systems,* vol. 2, no. 1, 2012.

[10] A. Altarawneh and R. Alrawashdeh, A multilayer implantable patch antenna based on spiral split rings, *2022 Intrnational Worjshop on Antenna Technology,* 2022.

[11] R. Alrawashdeh, Patch antenna based on spiral split rings for bone implants, PRZEGLĄD ELEKTROTECHNICZNY, no. 7, pp. 129-134, 2020.

[12] M. Matthaiou, S. Koulouridis and S. Kotsopoulos, A noval dual-band implantable antenna for pancreas telemetry sensor applications, *Telecom,* vol. 3, no.1, pp. 1-16, 2022.

[13] F. Merli, L. Bolomey, J. –F. Zurcher, E. Meurville and A. K. Skrivervik, Versatility and tunability of an implantable antenna for telemedicine, *Proceedings of the 5th European Conference on Antennas and Propagation. IEEE,* pp. 2487-2491, 2011.

[14] Y. Kamel and H. Mohamed, Miniaturized triple-band circular polarized implantable patch antenna for bio-telemetry applications, *IEEE Antennas and Wireless Propagation Letters,* vol. 22, no. 1, 2023.

[15] O. Celik and S. Basaran, Compact triple-band implantable antenna for multitasking medical devices, *Journal of Electrical Engineering,* vol. 73, no. 3, pp. 166-173, 2022.

[16] S. Das and D. Mitra, A compact wideband flexible implantable slot antenna design with enhanced gain, *IEEE Transactions on Antenna and Propagation*, vol. 66, no. 8, 2018.

[17] Y. Feng, P. Chen, S. Pan and G. Li, Ultra-wideband flexible implantable antenna for wireless capsule endscopy system with performance improvement, *The Applied Computational Electromagnetics Society Journal,* vol. 36, no. 6, 2021.

[18] M. Yousaf, I. Ben Mabrouk, M. Zada, A. Akram, Y. Amin, M. Nedil and H. Yoo, An ultra-miniaturized antenna with ultra-wide bandwidth characteristics for medical implants systems, *IEEE Access*, vol. 9, pp. 40086-40097, 2021.

[19] H. Dawood, M. Zahid, S. Shoaib and A. Hussain, High gain flexible antenna for biomedical applications, *Proc. Of the International Conference on Electrical, Communication and Computer Engineering*, 2020.

[20] S. Ahmad, A. Khabba, A. Ghaffar and X. –J. Li, A compact wideband flexible circularly polarized implantable antenna for biotelemetry applications, *In 2021 IEEE International Symposium on Antennas and Propagation and USNC-URSI Radio Science Meeting,* pp. 695-696, 2021.

[21] S. Ahmad, B. Manzoor, S. Naseer, N. Santos-Valdivia, A. Ghaffar and M. Abbasi, X-shaped slotted patch biomedical implantable antenna for wireless communication networks, *Wireless Communications and Mobile Computing*, 2022.

[22] F. Faisal, M. Zada, A. Ejaz, Y. Amin, S. Ullah and H. Yoo, Aminiaturized dual-band implantable antenna system for medical applications, *IEEE Transactions on Antenna and Propagation*, vol. 68, no. 2, 2020.

[23] F. Faisal and H. Yoo, Aminiaturized noval-shape dual-band antenna foe implantable applications, *IEEE Transactions on Antenna and Propagation*, vol. 67, no. 2, 2019.

[24] N. Abbas, S. Ullah, Z. Bashir, A. Basir and H. Yoo, Design and measurment of a minuscule-sized implantable antenna for brain-machine interfaces, *IEEE Access*, 2023.

[25] S. Mosavinejad, P. Rezaei, A. Khazaei and J. Shirazi, A triple-band spiral-shaped antenna for high data rate fully passive implantable devices, *AEU-International Journal of Electronics and Communications*, vol. 159, 2023.

[26] P. Kirtonia, M. F. Samad, M. K. Hosain and M. E. Hossain, Differentially fed compact triple-band antenna for implantable medical devices, *1st International Conference on Advances in Seience, Engineering and Robotics Technology*, 2019.

[27] M. Yousaf, I. Ben Mabrouk, F. Faisal, M. Zada, Z. Bashir, A. Akram, M. Nedil and H. Yoo, A compact conformal implanatble antenn with multitasking capabilites for ingestible capsule endscope, *IEEE Access*, vol. 8, 2020.

[28] R. Alrawashdeh, Y. Huang, M. Kod and A. Sajak, Broadband flexible implanatble loop antenna with complementry split ring resonators, IEEE Antennas and Wireless Propagation Letters, vol. 14, 2015.

[29] CST-Computer Simulation Technology, 2013. http://www.CST.com

[30] R. Alrawashdeh, Implantable Antennas for Biomedical Applications, University of Liverpool, 2015.

[31] D. Andreuccetti, R. Fossi and C. Petrucci: An Internet resource for the calculation of the dielectric properties of body tissues in the frequency range 10 Hz - 100 GHz. IFAC-CNR, Florence (Italy), 1997. Based on data published by C. Gabriel et al. in 1996. [Online]. http://niremf.ifac.cnr.it/tissprop/.

[32] M. Sadiku and J. Buck, Elements of electromagnetics, London: Mcgraw hill higher education, 2012.

[33] W. Hayt, J. Kemmerly and S. Durbin, Engineering Circuit Analysis, New York: McGraw-Hill, 2012.

[34] R. Kumar, L. Solankin and S. Singh, SAR analysis of antenna implanted inside homogeneous human tissue phantom, *6th International Conference on Signal Processing and Integrated Networks*, Noida, India, pp. 755-759, 2019.